Supporting Information

Extending Photo-induced Charge Separation Lifetimes by using Supramolecular Design: Guanine-Perylenediimide G-Quadruplex

*Yi-Lin Wu, Kristen E. Brown, and Michael R. Wasielewski**

Department of Chemistry and Argonne-Northwestern Solar Energy Research (ANSER) Center, Northwestern University, Evanston, Illinois 60208-3113, United States

E-mail: m-wasielewski@northwestern.edu

Table of Contents

1. Synthesis

Materials and general methods. Reagents were purchased at reagent grade and used as received. Flash column chromatography was carried out with SiO_2 (particle size 0.040–0.063 mm, 230–400 mesh) and technical solvents. ^{1}H and ^{13}C NMR spectra were measured on a Bruker AVANCE III 500, an AVANCE III 600, or a Varian Inova 500 instrument. Chemical shifts were reported in ppm relative to the signal of $Si(CH_3)_4$. Residual solvent signals in the NMR spectra were used as an internal reference. Coupling constants (*J*) were given in Hz. The apparent resonance multiplicity was described as s (singlet), d (doublet), t (triplet), and m (multiplet). ESI-MS spectra were measured on a Thermo Finnegan LCQ mass spectrometer, MALDI-MS spectra on a Bruker Autoflex III MALDI-TOF, and high-resolution HR-ESI-MS spectra on an Agilent 6210 LC-TOF; signals are reported in m/z units.

Scheme S1. **Synthesis of GPDI**.

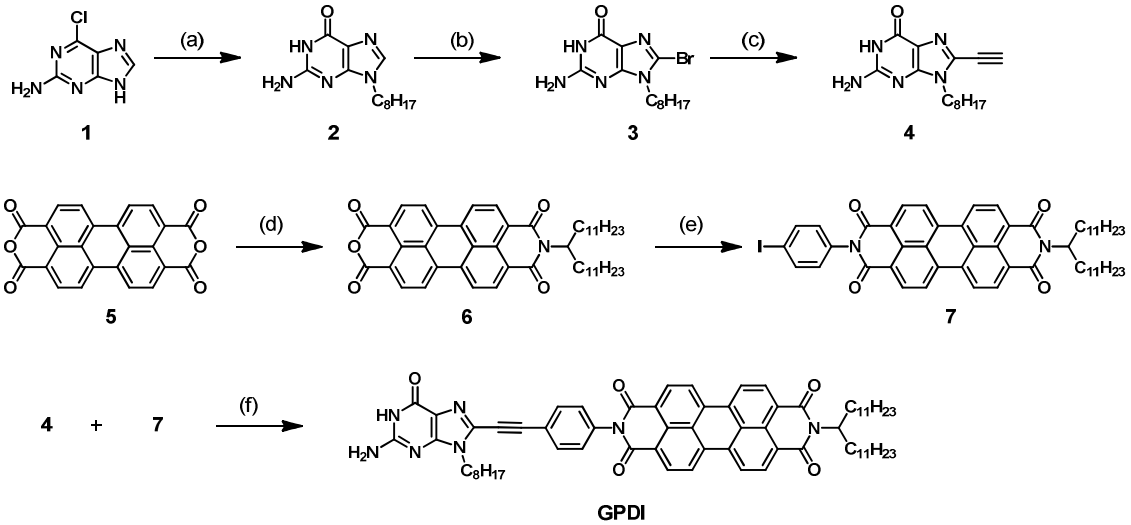

(a) 1-Bromooctane, K_2CO_3, *N*,*N*-dimethylformamide, r.t., 20 h, 72%; 0.5 M $HCl_{(aq)}$, reflux, 18 h, 95%. (b) *N*-Bromosuccinimide, MeCN, H_2O, r.t., 1.5 h, 77%. (c) Triisopropylsilyl acetylene, $Pd(PPh_3)_4$, CuI, *N*,*N*-dimethylformamide, Et_3N, 50 ºC, 40 h; nBu_4NF, THF, 2 h, r.t., 70%. (d) Tricosan-12-amine, imidazole, 160 ºC, 16 h; KOH, *t*BuOH, reflux, 2 h, 34%. (e) 4-Iodoaniline, zinc acetate, imidazole, 160 ºC, 3 h, 78%. (f) $Pd(PPh_3)_4$, CuI, *N*,*N*-dimethylformamide, Et_3N, 50 ºC, 18 h, 30%.

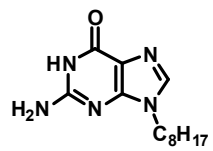

2

***N*^{9}-Octyl guanine (2-amino-9-octyl-1*H*-purin-6(9*H*)-one, 2).** The synthesis of compound **2** follows the reported procedure[1,2] for a similar material. A solution of 6-chloro-9*H*-purin-2-amine (5.0 g, 29.5 mmol), 1-bromooctane (5.7 g, 29.5 mmol), K_2CO_3 (6.11 g, 44.2 mmol), *N*,*N*-dimethylformamide (DMF, 100 mL) was stirred at room temperature (r.t.) for 20 h. DMF was removed on a rotary evaporator; flash column chromatography of the residue on SiO_2 (CH_2Cl_2 → CH_2Cl_2/MeOH 35:10) separated the N^6-octyl byproduct from the desired N^9-octyl product (6 g, 72%). The product (6 g, 21.3 mmol) from the above synthesis was suspended in aqueous HCl solution (0.5 M, 600 mL). The mixture was heated at reflux for 18 h. The cooled solution was neutralized (pH ~ 7) with NaOH pellets, and the title compound as white and fine precipitates were collected by filtration and washed with water (5.3 g, 20.2 mmol, 95%). ^{1}H NMR (500 MHz, DMSO-d_6, 25 ºC): δ = 10.54 (s, 1 H, (CO)NH), 7.70 (s, 1 H, C^8-H), 6.44 (s, 2 H, NH_2), 3.91 (t, J = 7.1 Hz, 2 H, NCH_2), 1.79–1.53 (m, 2 H, CH_2), 1.34–1.08 (m, 10 H, CH_2), 0.84 (t, J = 6.8 Hz, 3 H, CH_3); ^{13}C NMR (125 MHz, DMSO-d_6, 25 ºC): δ =156.79, 153.50, 151.13, 137.50, 116.42, 42.69, 31.19, 29.41, 28.61, 28.49, 26.00, 22.09, 13.99; ESI-MS: m/z 1075.457 ([4×*M*+Na]$^+$, calcd for $C_{52}H_{84}N_{20}NaO_4$: 1075.688), 549.283 ([2×*M*+Na]$^+$, calcd for $C_{26}H_{42}N_{10}NaO_2$: 549.338), 527.375 ([2×*M*+H]$^+$, calcd for $C_{26}H_{43}N_{10}O_2$: 527.356), 264.318 ([*M*+H]$^+$, calcd for $C_{13}H_{22}N_5O$: 264.182).

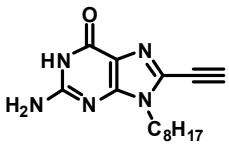

4

8-Ethynyl guanine (2-amino-8-ethynyl-9-octyl-1*H*-purin-6(9*H*)-one, 4). The synthesis of compound **4** follows the reported procedure[3] for a similar material. *N*-Bromosuccinimide (4.06 g, 22.8 mmol) was added in 10 portions to the suspension of **2** (4.00 g, 15.2 mmol) in MeCN (150 mL) and H_2O (40 mL) at r.t. over 30 min. The mixture was further stirred at r.t. for 1 h. MeCN was removed on a rotary evaporator,

and the precipitates were collected by filtration and washed with water (**3**, 4 g, 11.7 mmol, 77%). A mixture of **3** (2.00 g, 5.84 mmol), triisopropylsilyl acetylene (5.24 mL, 24 mmol), $Pd(PPh_3)_4$ (330 mg, 0.29 mmol), CuI (110 mg, 0.58 mmol) in DMF (100 mL) and Et_3N (45 mL) was heated at 50 ºC for 40 h under N_2. The solvents were removed on a rotary evaporator; flash column chromatography of the residue on SiO_2 (CH_2Cl_2 → CH_2Cl_2/MeOH 20:1) yielded the silyl-protected ethynyl precursor for **4**. This material was subsequently dissolved in THF (100 mL) and MeOH (5 mL), and treated with nBu$_4$NF (1 M solution in THF, 10 mL, 10 mmol) at 0 ºC. The mixture was stirred at r.t. for 1 h. Solvents were removed on a rotary evaporator; flash column chromatography of the residue on SiO_2 (CH_2Cl_2/MeOH 20:1 → 20:1.5) yielded **4** as a white solid (1.18 g, 4.1 mmol, 70%). ^{1}H NMR (500 MHz, DMSO-d_6, 25 ºC): δ = 10.69 (s, 1 H, (CO)NH), 6.61(s, 2 H, NH_2), 4.74 (s, 1 H, C≡CH), 3.96 (t, J = 7.0 Hz, 2 H, NCH_2), 1.64–1.74 (m, 2 H, CH_2), 1.16–1.31 (m, 10 H, CH_2), 0.84 (t, J = 6.9 Hz, 3 H, CH_3); ^{13}C NMR (125 MHz, DMSO-d_6, 25 ºC): δ =156.27, 154.23, 151.01, 129.23, 116.60, 84.97, 73.66, 42.71, 31.17, 28.95, 28.56, 28.46, 25.91, 22.09, 13.99; ESI-MS: m/z 1171.634 ([4×M+Na]$^+$, calcd for $C_{60}H_{84}N_{20}NaO_4$: 1171.688), 288.309 ([M+H]$^+$, calcd for $C_{15}H_{22}N_5O$: 288.182).

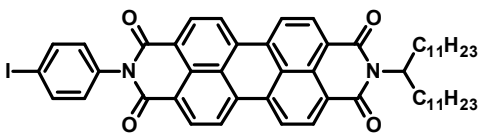

7

***N*-(4-Iodophenyl)-*N*′-(tricosan-12-yl)-perylene-3,4,9,10-bis(dicarboximide) (7).** The synthesis of compound **7** follows the reported procedure[4] for a similar material. A mixture of *N*-(tricosan-12-yl)-perylene-3,4-dicarboxyanhydride-9,10-dicarboximide[5] (**6**, 200 mg, 0.27 mmol), 4-iodoaniline (177 mg, 0.81 mmol), zinc acetate dihydrate (25 mg, 0.14 mmol), and imidazole (2 g) was heated at 160 ºC for 3 h under N_2. The cooled mixture was dissolved in CH_2Cl_2, and the organic solution was washed with 2 N HCl. Purification by flash

chromatography (SiO_2; CH_2Cl_2/hexanes 8:1 → CH_2Cl_2) of the concentrated organic phase afforded the title compound as a red solid (195 mg, 0.21 mmol, 78%). ^{1}H NMR (500 MHz, $CDCl_3$, 25 ºC): δ = 8.48–8.54 (m, 4 H, PDI-H), 8.28–8.32 (m, 4 H, PDI-H), 7.87 (d, J = 8.4 Hz, 2 H, phenylene), 7.15 (d, J = 8.4 Hz, 2 H, phenylene), 5.11–5.18 (m, 1 H, NCH), 2.19–2.27 (m, 2 H, CH_2), 1.87–1.95 (m, 2 H, CH_2), 1.15–1.38 (m, 36 H, CH_2), 0.83 (t, J = 6.9 Hz, 6 H, CH_3); ^{13}C NMR (125 MHz, $CDCl_3$, 25 ºC): δ = 162.93, 138.56, 134.63, 131.35, 130.62, 129.26, 129.07, 126.01, 125.77, 123.03, 122.74, 122.70, 94.67, 54.90, 32.29, 31.86, 29.62, 29.60, 29.56, 29.55, 29.30, 27.07, 22.63, 14.09; MALDI-MS: m/z 913.867 ([M]$^-$, calcd for $C_{53}H_{59}IN_2O_4$: 914.352).

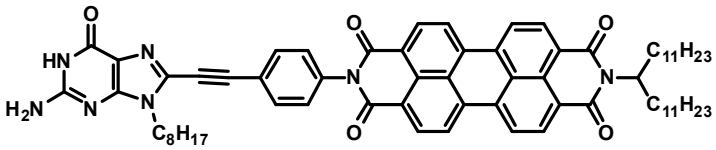

GPDI

Guanine–PDI conjugate (GPDI). A suspension of 8-ethynyl guanine **4** (78 mg, 0.27 mmol) and iodo-PDI **7** (300 mg, 0.33 mmol) in DMF (50 mL) and Et_3N (5 mL) was purged with N_2 for 20 min, charged with $Pd(PPh_3)_4$ (30 mg, 0.025 mmol) and CuI (10 mg, 0.05 mmol), and purged again with N_2 for 20 min. The mixture, which turned into a homogeneous solution during the course of the reaction, was heated at 50 ºC for 18 h under N_2. The solvents were removed on a rotary evaporator; flash column chromatography of the residue on SiO_2 ($CHCl_3$/MeOH 20:1 → 15:1) yielded **GPDI** as a red solid (97 mg, 0.09 mmol, 30%). Further trituration of the solid with Et_2O removed the red and fluorescent impurity. ^{1}H NMR (500 MHz, DMSO-d_6, 100 ºC): δ = 10.43 (s, 1 H, (CO)NH), 8.95–8.78 (m, 4 H, PDI-H), 8.65–8.46 (m, 4 H, PDI-H), 7.79 (d, J = 8.4 Hz, 2 H, phenylene), 7.55 (d, J = 8.4 Hz, 2 H, phenylene), 6.35 (s, 2 H, NH2), 5.21–4.94 (m, 1 H, NCH), 4.14 (t, J = 7.1 Hz, 2 H, NCH_2), 2.30–2.14 (m, 2 H, CH_2), 1.83–1.91 (m, 4 H, CH_2), 1.43–1.10 (m, 46 H, CH_2), 0.86 (t, J = 6.8 Hz, 3 H, CH_3), 0.80 (t, J = 6.8 Hz, 6 H, CH_3). MALDI-MS: m/z 1074.549

(positive polarization, $[M+H]^+$, calcd for $C_{68}H_{80}N_7O_5$: 1074.622), 1073.183 (negative polarization, $[M]^-$, calcd for $C_{68}H_{79}N_7O_5$: 1073.615); HR-ESI-MS: m/z 1074.624 ($[M+H]^+$, calcd for $C_{68}H_{80}N_7O_5$: 1074.622). The strong association (H-bonding and π-stacking) of **GPDI** prohibits recording the ^{13}C NMR spectrum.

2. Steady-state UV-Vis Spectra of GPDI (Monomer and G-quadruplex)

The steady-state absorption spectra of the monomer or G-quadruplex of **GPDI** in THF were measured on a Shimadzu 1601 UV-Vis spectrometer, and shown in Figure S1. Based on the relative intensity of the vibronic absorptions A_{0-0}/A_{0-1}, it was found that association of **GPDI** is negligible in THF (*i.e.* monomeric **GPDI**) at low concentrations (< 10^{-4} M). The absorption spectrum of the **GPDI**-quadruplex solution containing 3×10^{-3} M **GPDI** and 0.25 eq. KPF_6 was measured in a 100 μm-path cuvette, and is consistent with *H*-aggregation of the PDI moieties.

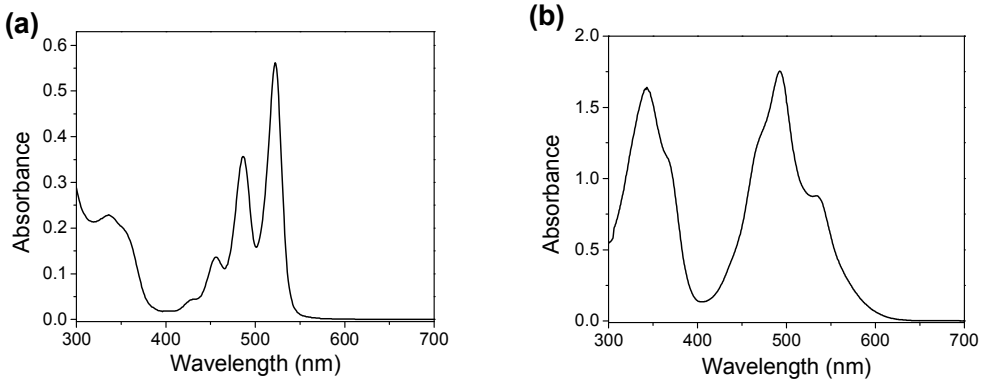

Figure S1. Steady-state absorption spectra of (a) monomeric **GPDI** ($c \sim 10^{-5}$ M) and (b) **GPDI**-quadruplex ($c = 3 \times 10^{-3}$ M, 0.25 eq. KPF_6) in THF.

3. Diffusion-ordered NMR Spectra of $(GPDI)_8$

The hydrodynamic radii (r) of (spherical) molecules can be, in principle, evaluated by the Stokes-Einstein equation, $D = kT/6\pi\eta r$, where D is the diffusion coefficient, k the Boltzmann constant, T the temperature, and η the viscosity of the solution, which is often approximated by that of the solvent. The diffusion coefficient of G-quadruplex $(\mathbf{GPDI})_n$ was estimated by NMR diffusion-ordered spectroscopy (DOSY) experiments on a Bruker AVANCE III 600 MHz spectrometer at 298 K. The convection compensated *dstebpgp3s* pulse program,[6,7] with double stimulated echo for convection compensation and LED (longitudinal eddy delay) bipolar gradient pulses for diffusion, was employed. Since DOSY spectra often include artifacts resulting from convection, viscosity change, and fluctuation of the sample position and temperature, an accurate estimation of D is found difficult. Tetramethylsilane (TMS) was hence added as an internal standard,[8] and the hydrodynamic radius of G-quadruplex $(\mathbf{GPDI})_n$ was calculated by comparing its diffusion coefficient to that of TMS (D_{TMS}).[8]

A series of one-dimensional ^1H spectra of $(\mathbf{GPDI})_n$ was recorded by applying gradient pulses of varied strengths (Figure S2). Signals of the small molecules (THF, H_2O, and TMS) diminished significantly by small dephasing gradients, due to their longer mean free paths of diffusion. Diffusion coefficient of each molecule was calculated (Bruker TopSpin™ 2.1) according to how the intensity of the characteristic resonance changes with respect to the gradient strength. The diffusion coefficient of $(\mathbf{GPDI})_n$ ($D_{(GPDI)n} \sim 1.8\times10^{-10}$ m^2s^{-1}) was found 14±1 times smaller than D_{TMS} (*ca.* 24.7×10^{-10} m^2s^{-1}), and the radius of $(\mathbf{GPDI})_n$ $r_{(GPDI)n} = r_{TMS} \times [D_{TMS}/D_{(GPDI)n}] \sim 29$ Å was estimated ($r_{TMS} = 2.1$ Å).[8]

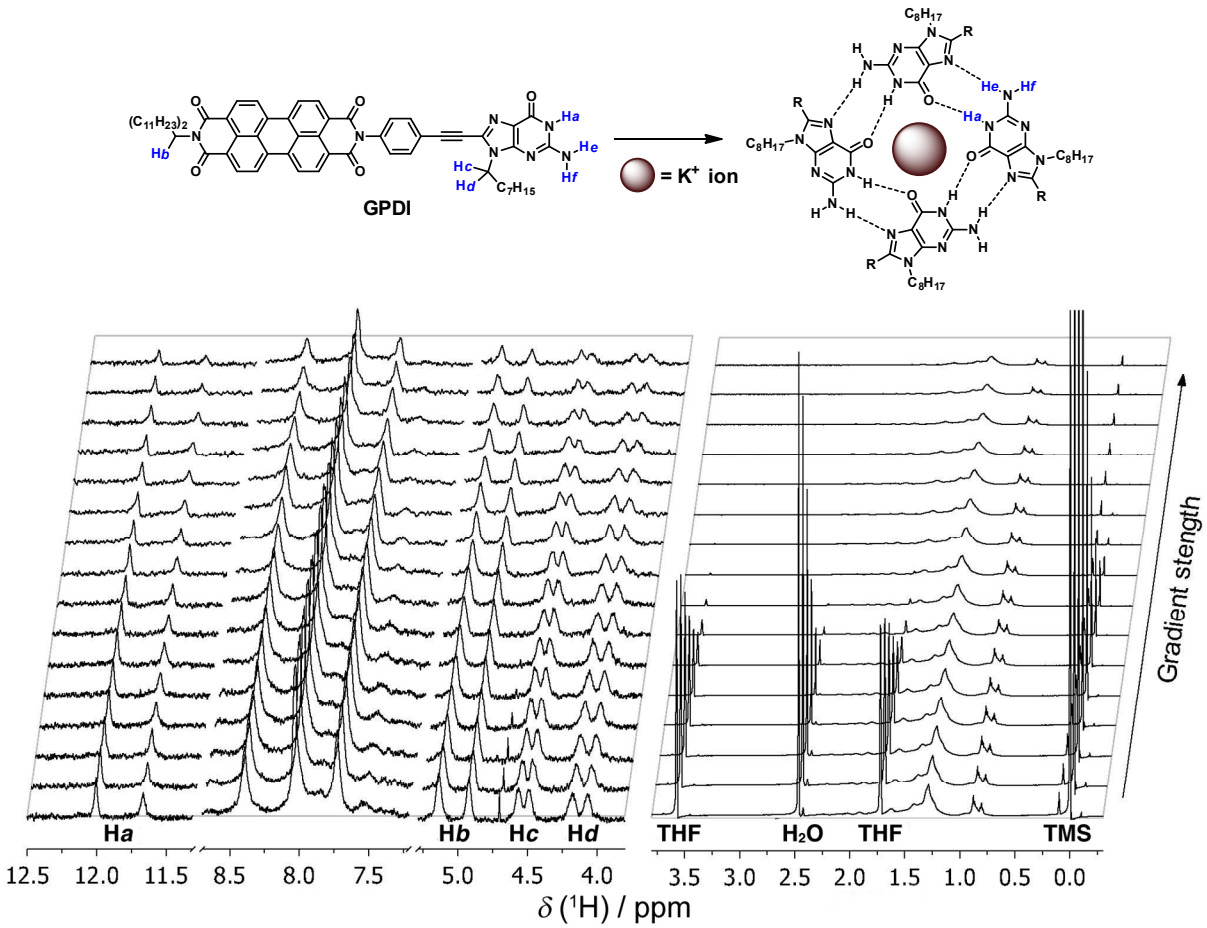

Figure S2. A stack of ^{1}H NMR (THF-d_8, 600 MHz) of **GPDI** (3×10^{-3} M + 0.25 equiv. KPF_6) recorded at different strengths of gradient pulses; signal assignments are given. The signal intensities in the region of 3.8–12.5 ppm were magnified.

4. X-ray Scattering Measurements and Analysis

Structural studies on **GPDI**-quadruplex in THF at room temperature were performed using the high-flux synchrotron source at beamline 12-ID-C of the Advanced Photon Source at Argonne National Laboratory. The sample was placed in a 2 mm quartz capillary with a wall thickness of 0.2 mm. The X-ray scattering instrument employed a double-crystal Si(111) monochromator and a two-dimensional mosaic CCD detector. Scattering intensity is a function of the modulus of the scattering vector q, related to the scattering angle 2θ by the equation $q = (4\pi/\lambda)\sin\theta$, where λ is the X-ray wavelength. Samples were examined by adjusting the sample-to-detector distance to measure across two detection ranges of q, 0.006 to 0.3 $Å^{-1}$ and 0.1 to 1.6 $Å^{-1}$.

Chart S1. Possible G-quadruplex of **GPDI** (Potassium Ions are Omitted for Clarity).

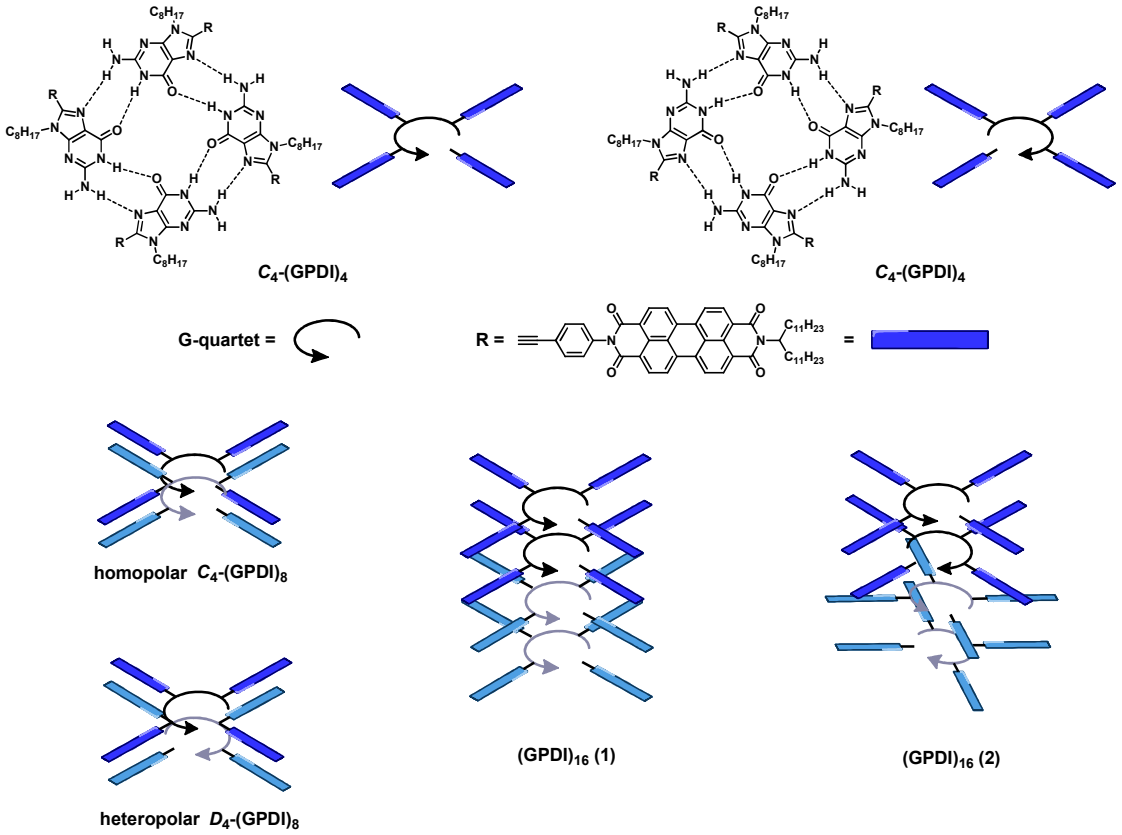

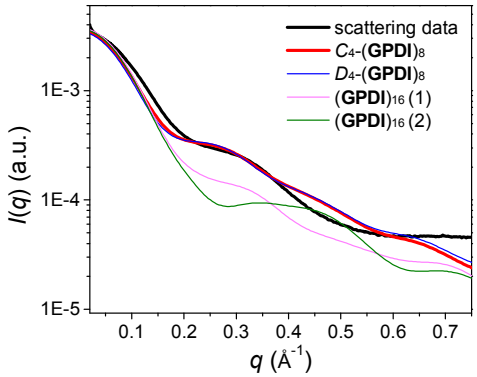

Figure S3. Comparison of the experimental scattering intensity for **GPDI**-quadruplex with the simulated scattering intensity for the structural models.

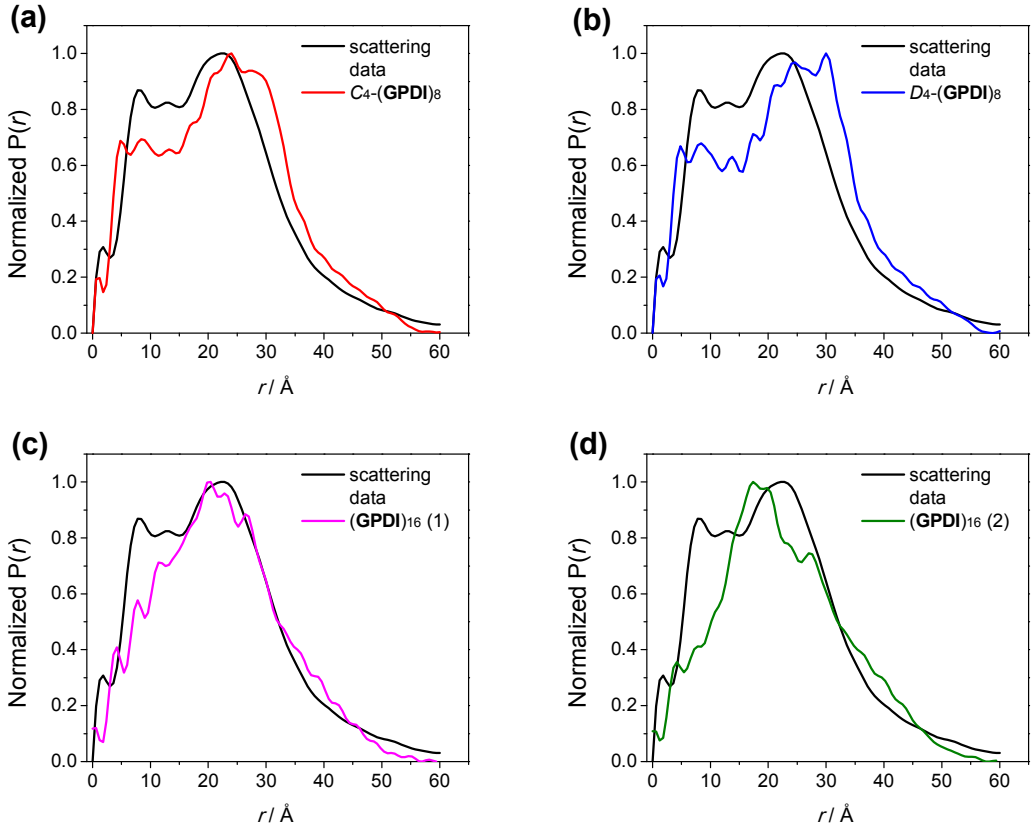

Figure S4. Comparison of the pair distribution functions (PDFs) generated from the scattering data with those from the structural models. See Chart S1 for the geometries of (a) C_4-(**GPDI**)$_8$, (b) D_4-(**GPDI**)$_8$ (c) (**GPDI**)$_{16}$ (1), and (d) (**GPDI**)$_{16}$ (2).

Four possible geometries (among many others) of **GPDI** G-quadruplexes were examined. They differ from each other in terms of the size and the relative orientation and "polarity"[9] of the neighboring hydrogen-bonded G-quartets (Chart S1). Geometry of each G-quadruplex was optimized by molecular-mechanic calculations (MMFF94s for the K^+-free geometries first, followed by UFF for the K^+-included full structures).[10] The simulated scattering intensity and the corresponding pair-distance distribution function (PDF) were generated based on the "alkyl-chain deleted" geometries, and overlaid in Figure 3b in the main text and shown here in Figure S3 (scattering intensity) and S4 (PDF) for clarity. The aliphatic substituents were disregarded in the analysis of scattering data, since the contrast of the electron densities between these motifs and solvents is low. Notice (i) the similarity in PDFs between the two 8-mers and between the two 16-mers, and (ii) the roughly bell-shaped PDFs for the two 16-mers, which reflect the nearly globular geometries of these aggregates.

There remains, however, ambiguity about the Nα–Cβ–Cγ–Cδ dihedral angle in G-quadruplexes by SAXS/WAXS study (Figure S5). For instance, the PDFs of two rotational isomers of C_4-(**GPDI**)$_8$, where the Nα–Cβ–Cγ–Cδ angle is close to 0° in one ("planar") and 90° in another ("twisted"), are virtually indistinguishable.

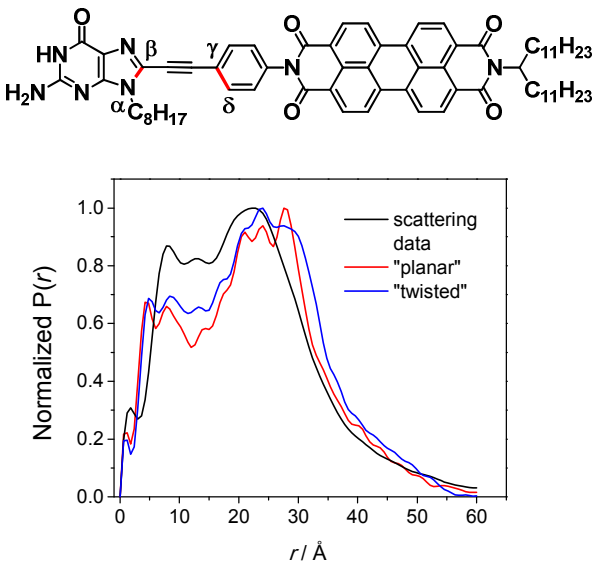

Figure S5. Comparison of the pair distribution functions (PDFs) between two C_4-(**GPDI**)$_8$ isomers, where the Nα–Cβ–Cγ–Cδ dihedral angle is close to 0° ("planar") in one and 90° ("twisted") in another.

While the hydrodynamic radius R_h ~ 29 Å was obtained by the DOSY experiment, the radius of gyration (R_g) is about 15.1 Å by Guinier analysis of the scattering data [$\ln I(q) = \ln I_o - q^2 R_g^2/3$], or 16.5 Å according to the associated pair-distance distribution function [$R_g^2 = {}^1/_{2N^2} \sum_j^N \sum_i^N (r_{ij})^2$, where r_{ij} is inter-atomic distance] (Table S1).

Table S1. Comparison of the Characteristic Radius of **GPDI**-quadruplex.

	R_h	R_g (Guinier)	R_g (PDF)	R_g (columnar)
C_4 (**GPDI**)$_8$	29 Å	15.1 Å	16.5 Å	17.7 Å

The apparently smaller number for R_g is partly resulted from the low contrast between the solvent and the flexible alkyl chain on the periphery of the G-quadruplex. These R_g values are

consistent with the number of 17.7 Å calculated by $R_g^2 = (R^2/2 + h^2/12)$ for a columnar object, where h ~ 3.4 Å is the height of the quadruplex and R ~ 25 Å is the distance from the center of each G-quartet to the outer imide nitrogen (homogeneous density assumed). The larger value for R_h, additionally, is related to the detailed solvation of the solutes that influences the translational dynamics of the segments of the alkyl groups.[11,12]

5. Transient Absorption

Femtosecond (fs) transient absorption experiments were performed on **GPDI** monomer (*ca*. 10^{-5} M) and G-quadruplex (3×10^{-3} M + 0.25 equiv. KPF_6) in THF using instrumentation previously described.[13] The output of a 4 W 1 KHz Ti:sapphire regenerative amplifier (Spitfire Pro, Spectra Physics) generates visible excitation pulses (490 and 525 nm) and a broadband fs-probe pulse. The Gaussian instrument response determined by optical Kerr effect cross-correlation measurements has a full-width half-max of *ca*. 200 fs. A 2-mm quartz cuvette was used to hold the monomeric **GPDI** sample in THF, resulting in an optical density of ~0.5. The high concentration of **GPDI**-quadruplex, kept at the same concentration as the NMR and SAXS/WAXS samples, necessitated a path-length of 100 μm. Transient spectra of both samples were acquired from 0 to7 ns with 3 s averaging at each time delay and 4 scans.

In addition to the experiments described in the main text, a nearly saturated THF solution (4.4×10^{-4} M, in a 100 μm cell; the solution is apparently cloudy at higher concentration) of **GPDI** was excited at 525 nm to examine whether the long-live charge separation can be observed in the concentrated **GPDI** solution. The femtosecond time-resolved absorption spectra of this sample exhibits the decay of the excited state in τ = 17 ps (Figure S6a), similar to the kinetics observed in the monomer sample (10^{-5} M, Figure 4a).

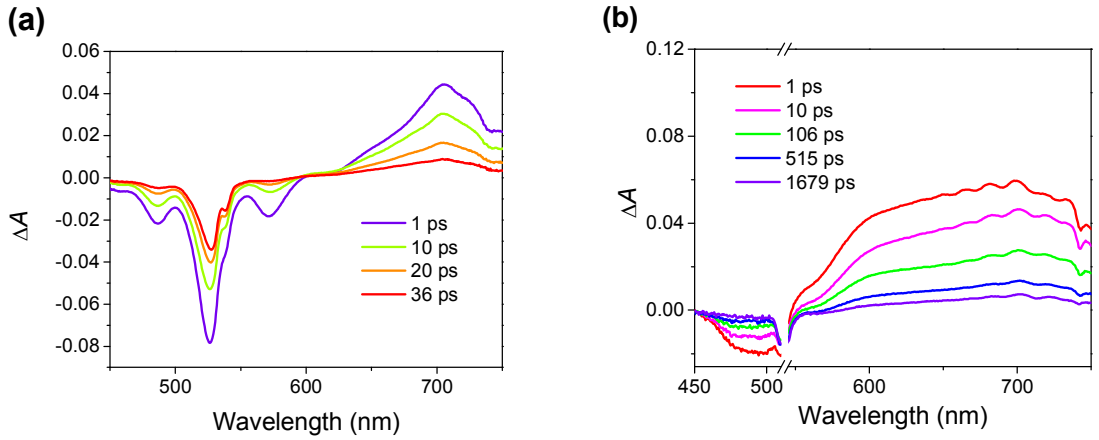

Figure S6. Femtosecond time-resolved absorption spectra of (a) the nearly saturated THF solution of **GPDI** (0.4×10^{-3} M) and (b) the G-quadruplex at 525 nm.

For **GPDI**-quadruplex, shifting the excitation pulse to 525 nm (0.5 μJ/pulse) reveals the broad transient absorption at 600–750 nm (Figure S6b, decay time constants of 77 and 1121 ps, similar to the results observed by excitation at 470 nm). Excitation at 525 nm, however, prohibits the observation of the absorption at 520 nm. This 520 nm peak, along with the broad-band absorption, suggests the formation of radical anion of dimeric PDI ($PDI_2^{-\bullet}$). Comparable transient absorption features have been observed in the radical anion of dimeric 1,7-bis(phenoxy) PDI, where the corresponding peak was noticed around 550 nm.[14,15]

6. Electrochemistry

Measurements were performed with a CH Instruments Model 622 electrochemical workstation. All experiments were carried out at ambient temperature in THF containing 0.1 M nBu$_4$NPF$_6$ in a three-electrode cell by cyclic voltammetry (CV; scan rate 0.1 V s^{-1}) and differential pulse voltammetry (DPV). The working electrode was a platinum disk (2 mm in diameter) or a glassy-carbon (GC) disk (3 mm), the auxiliary electrode a Pt wire, and the reference electrode Ag/AgCl. Potentials are given relative to saturated calomel electrode (SCE).

Table S2. Cyclic Voltammetry (CV) and Differential Pulse Voltammetry (DPV) Data in THF.[a]

	CV[b]		DPV
	E_{pc}/V[c]	E^o/V	$E_{1/2}$ /V
monomer	–0.54	–0.49	–0.51
	–0.84	–0.80	–0.80
quadruplex	–0.47	–0.41[d]	–0.38
	–0.60	–0.52[d]	–0.50
	–0.91		–0.78
			–1.45
	–1.68		–1.58

[a] Potentials are given relative to saturated calomel electrode (SCE); working electrode = Pt disk, counter electrode = Pt wire, reference electrode = Ag/AgCl, supporting electrolyte 0.1 M n-Bu$_4$NPF$_6$. [b] CV scan rate = 0.1 V s^{-1}. [c] Cathodic peak potential. [d] Scan range = 0 to –0.75 V.

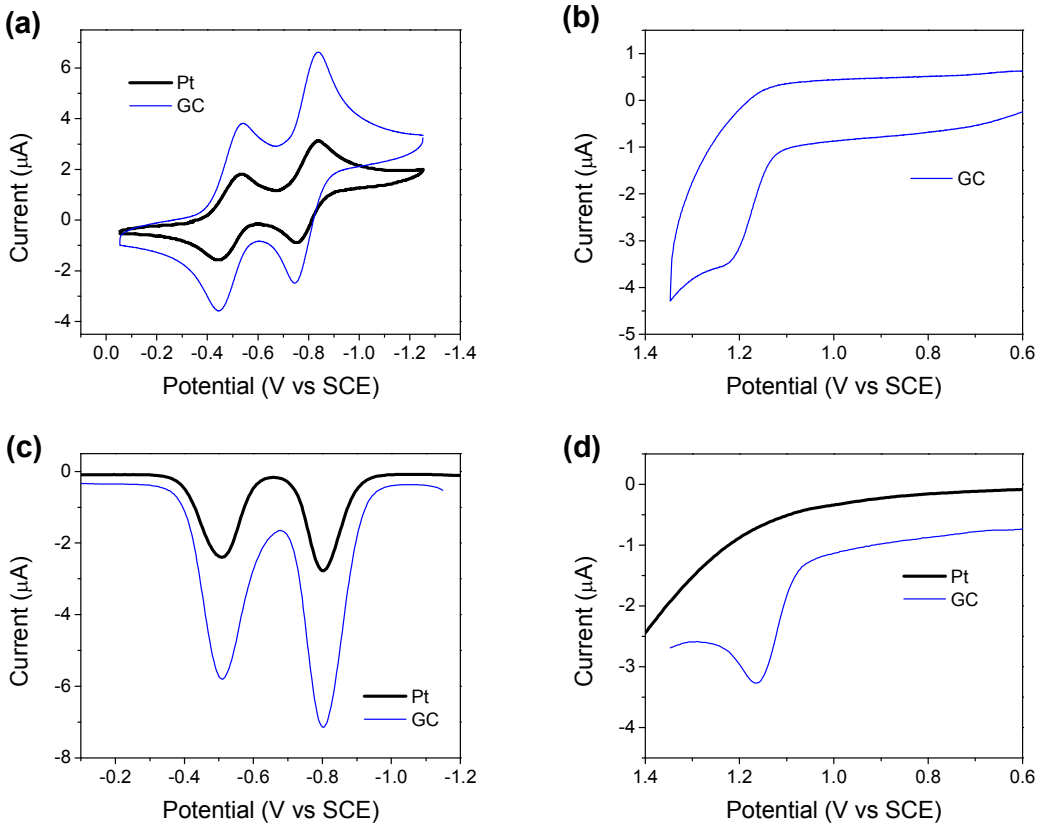

Figure S7. Electrochemical voltammograms for **GPDI** monomer in THF ($c = 3.7 \times 10^{-4}$ M). (a) CV from 0 to –1.2 V, (b) CV from 0.6 to 1.4 V, (c) DPV from 0 to –1.2 V, and (d) DPV from 0.6 to 1.4 V. Working electrode used in each measurement is indicated in the plot legend.

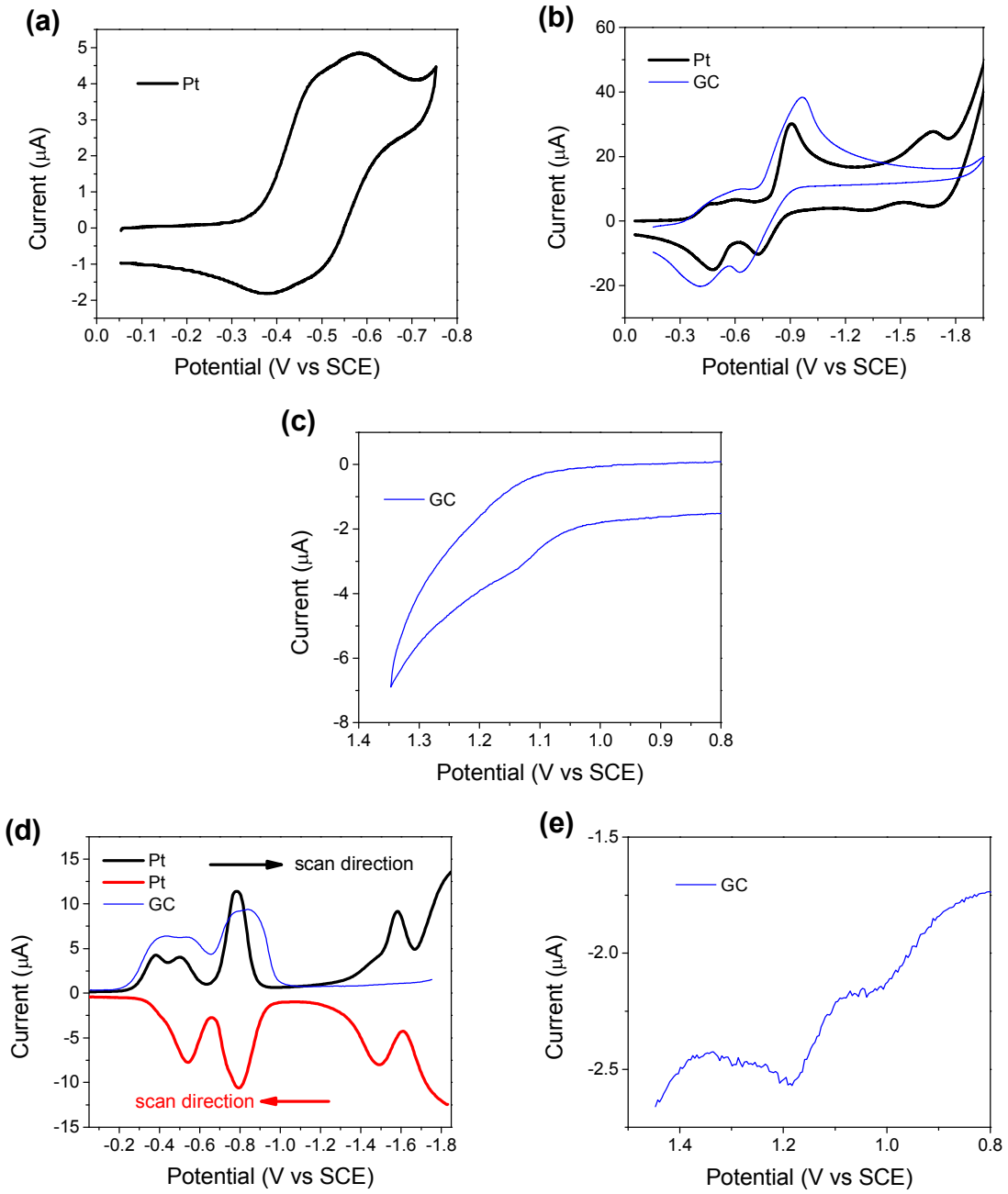

Figure S8. Electrochemical voltammograms for $(\mathbf{GPDI})_8$ quadruplex in THF ($c_{(\mathbf{GPDI})} = 3.7 \times 10^{-3}$ M with 0.25 eq. KPF_6). (a) CV from 0 to –0.75 V, (b) CV from 0 to –1.85 V, (c) CV from 0.8 to 1.4 V, (d) DPV from 0 to –1.8 V with scan directions shown, and (e) DPV from 0.8 to 1.4 V. Working electrode used in each measurement is indicated in the plot legend.

In brief, with a GC electrode, we found that the reduction potentials of the **GPDI** monomer and the corresponding G-quadruplex are identical to the numbers obtained with a Pt electrode. The reduction of the latter occurs at 100 mV more positive than the former, a result found with both the Pt and GC electrodes. On the oxidation side, with a GC electrode, we are able to observe an oxidation wave for the **GPDI** monomer at +1.17 V vs. SCE; however, observation of the corresponding oxidation wave for the **GPDI**-quadruplex is still difficult. Although the oxidation of **GPDI**-quadruplex also seems to take place more easily than the monomer, the very small oxidative current found for the quadruplex (> 50 times smaller than its reductive current under the same conditions) suggests different adsorptive behaviors of the monomer and the G-quadruplex toward the GC (and Pt) electrode during the oxidative scan. Therefore, no definitive comparison of oxidation potentials can be made here.

7. References

(1) Harnden, M. R.; Jarvest, R. L.; Bacon, T. H.; Boyd, M. R. *J. Med. Chem.* **1987**, *30*, 1636-1642.

(2) Hanna, N. B.; Bhattacharya, B. K.; Robins, R. K.; Avery, T. L.; Revankar, G. R. *J. Med. Chem.* **1994**, *37*, 177-183.

(3) González-Rodríguez, D.; Janssen, P. G. A.; Martín-Rapún, R.; De Cat, I.; De Feyter, S.; Schenning, A. P. H. J.; Meijer, E. W. *J. Am. Chem. Soc.* **2010**, *132*, 4710-4719.

(4) Langhals, H.; Poxleitner, S.; Krotz, O.; Pust, T.; Walter, A. *Eur. J. Org. Chem.* **2008**, 4559-4562.

(5) Giaimo, J. M.; Lockard, J. V.; Sinks, L. E.; Scott, A. M.; Wilson, T. M.; Wasielewski, M. R. *J. Phys. Chem. A* **2008**, *112*, 2322-2330.

(6) Jerschow, A.; Müller, N. *J. Magn. Reson.* **1997**, *125*, 372-375.

(7) Jerschow, A.; Müller, N. *J. Magn. Reson.* **1998**, *132*, 13-18.

(8) González-Rodríguez, D.; van Dongen, J. L. J.; Lutz, M.; Spek, A. L.; Schenning, A. P. H. J.; Meijer, E. W. *Nat. Chem.* **2009**, *1*, 151-155.

(9) Masiero, S.; Trotta, R.; Pieraccini, S.; De Tito, S.; Perone, R.; Randazzo, A.; Spada, G. P. *Org. Biomol. Chem.* **2010**, *8*, 2683-2692.

(10) Hanwell, M. D.; Curtis, D. E.; Lonie, D. C.; Vandermeersch, T.; Zurek, E.; Hutchison, G. R. *J. Cheminfo.* **2012**, *4*.

(11) Tsunashima, Y.; Hirata, M.; Nemoto, N.; Kurata, M. *Macromolecules* **1987**, *20*, 1992-1999.

(12) Konishi, T.; Yoshizaki, T.; Yamakawa, H. *Macromolecules* **1991**, *24*, 5614-5622.

(13) Brown, K. E.; Veldkamp, B. S.; Co, D. T.; Wasielewski, M. R. *J. Phys. Chem. Lett.* **2012**, *3*, 2362-2366.

(14) Sinks, L. E.; Rybtchinski, B.; Iimura, M.; Jones, B. A.; Goshe, A. J.; Zuo, X. B.; Tiede, D. M.; Li, X. Y.; Wasielewski, M. R. *Chem. Mater.* **2005**, *17*, 6295-6303.

(15) van der Boom, T.; Hayes, R. T.; Zhao, Y.; Bushard, P. J.; Weiss, E. A.; Wasielewski, M. R. *J. Am. Chem. Soc.* **2002**, *124*, 9582-9590.